J Solid State Electrochem
DOI 10.1007/s10008-016-3442-x

ORIGINAL PAPER

Size-dependent photocurrent switching in chemical bath deposited CdSe quantum dot films

M. V. Malashchonak[1] · E. A. Streltsov[1] · A. V. Mazanik[1] · A. I. Kulak[2] · M. B. Dergacheva[3] · K. A. Urazov[3] · V. V. Pilko[1]

Received: 21 September 2016 / Revised: 13 October 2016 / Accepted: 18 October 2016

Abstract Size-dependent photocurrent switching has been investigated in chemical bath deposited CdSe quantum dot (QD) films with band gaps 2.26, 2.09, and 1.81 eV (corresponds to nanoparticles' average diameter of 4, 5, and 10 nm). CdSe films generate only anodic photocurrent (exhibit *n*-type semiconductor behavior) in the solution which contains only acceptor of photoholes (SO_3^{2-} anions), whereas cathodic photocurrent (corresponding to *p*-type behavior) arises after immersion of the films in polyselenide electrolyte (containing Se_n^{2-}/Se^{2-} redox system). Appearance of the cathodic photocurrent is related to chemisorptions of Se^{2-} and Se_n^{2-} anions, as revealed by the cadmium underpotential deposition (UPD). Photocurrent switching from anodic to cathodic becomes more pronounced with decreasing of CdSe nanoparticle size because small quantum dots with their broadened band gaps have more favorable conduction band energy for electron injection to polyselenide anions. On the contrary, particle size does not play a significant role for the injection of photoholes into the electrolyte because the position of the valence band is weakly size-dependent, and anodic photocurrent is determined primarily by the real surface area of the electrode, which was found to be greater than the geometrical one by 1–2 orders of magnitude from cadmium UPD. Effective charge separation at the highly developed CdSe-electrolyte interface contributes to high incident photon-to-current conversion efficiency of photocurrent (IPCE ~40 %).

Keywords CdSe · Quantum dots · Chemical bath deposition · Photocurrent switching · Underpotential deposition

✉ M. V. Malashchonak
che.malasche@gmail.com

[1] Belarusian State University, Nezalezhnastsi Av. 4, 220030 Minsk, Belarus

[2] Institute of General and Inorganic Chemistry, National Academy of Sciences of Belarus, Surganov St. 9/1, 220072 Minsk, Belarus

[3] Sokolsky Institute of Fuel, Catalysis and Electrochemistry, Almaty, Kazakhstan

Introduction

In recent decades, there has been a great interest in the study of physical, chemical, and optical properties of semiconductor nanocrystals (or quantum dots, QDs), in particular, cadmium selenide CdSe [1–11]. It is caused by numerous potential applications of this semiconductor: photovoltaics [1–5], photocatalysis [6–9], and optoelectronics [10, 11]. CdSe QDs have been employed in three different types of quantum dot solar cells: (i) quantum dot-sensitized solar cells, (ii) polymer hybrid solar cells, and (iii) metal junction solar cells [12]. By changing the size of CdSe QDs, one can not only vary the spectral sensitivity of solar cells but also improve their efficiency.

Chemical bath deposited (CBD) CdSe QDs usually form highly porous films which consist of a "network" of nanoparticles, display a blue shift in absorption spectra, and splitting of the bands into discrete levels as the QD size decreases [13, 14]. Such films possess a number of characteristics that distinguish them from the films obtained by other methods (e.g., using colloidal QDs). CBD CdSe films are characterized by an intimate contact between neighboring nanocrystals, which promotes charge transport over them [13]. At the same time, the porosity of the films allows the majority of nanoparticles to contact with the electrolyte. As a result, these films operate due to charge separation at the semiconductor-electrolyte interface rather than by a built-in space charge region as

Published online: 25 October 2016

normally occurs in photoelectrochemical (PEC) cells with bulk semiconductor [15, 16].

The type of PEC behavior of CdSe QDs is determined by what charges are moving into the solution: if the components of electrolyte capture photoholes, the anodic photocurrent is observed (oxidation of a reducing agent in the solution) [15]. In this case, photoelectrons move through the QDs into the conductive substrate, which corresponds to the *n*-type behavior. The cathodic photocurrent (*p*-type behavior) for the QDs is less common, because holes are characterized by significantly lower mobility, which increases the probability of recombination during their transfer to the conductive substrate. Hodes and coworkers have shown that treating of CdSe QDs surface in dilute HCl changes their PEC behavior from *n*-type like to *p*-type like, which is caused by surface modification-induced changes in the kinetics of charge transfer to the polysulfide electrolyte [13, 15]. The surface photovoltage spectroscopy shows that the CdSe QD films exhibit *p*-type properties after etching only in a humid ambient, whereas in a dry ambient they are *n*-type-like [17]. This fact indicates that the dominating type of surface traps (hole or electron) depends on the ambient. It was also suggested that the change in the type of CdSe QDs PEC behavior can be associated with enrichment of nanoparticles surface with selenium atoms [17]. Nevertheless, factors affecting the photocurrent sign, as well as quantum efficiency of PEC processes in CdSe QD films are still not completely clear.

Therefore, the purposes of this study were as follows: (i) to investigate the PEC behavior changes of CdSe QD films from *n*-type like to *p*-type like caused by formation of Se-terminated surface; (ii) to clarify the influence of CdSe nanoparticles size on photocurrent switching effect; (iii) to reveal factors determining efficiency of PEC processes in the CBD CdSe QD films.

Experimental section

Chemical deposition of CdSe QD films was carried out as described in [13–15]. FTO conductive glass was used as substrate for electrochemical measurements, and glass without FTO—for optical absorption, X-ray diffraction (XRD), Rutherford backscattering, Raman, and photoluminescence (PL) experiments. The films were deposited from an aqueous solution containing 80 mM Na_2SeSO_3 (0.2 mol of black selenium powder dissolved in 0.5 M Na_2SO_3 at 65 °C), 80 mM $CdSO_4$, and 150–170 mM potassium nitrilotriacetate $N(CH_2COOK)_3$ as a complexing agent. The pH of the solution was adjusted to 10.0 with 2 % KOH. CdSe film deposition was carried out in the dark at three different solution temperatures 3, 30, and 80 °C. These films will be denoted as CdSe(3), CdSe(30), and CdSe(80), respectively. According to [13–15], an increase in temperature of the solution increases the size of the CdSe particles, as well as the deposition rate. In order to obtain a comparable thickness of the films grown at different temperatures, deposition time was chosen equal to 40, 18, and 14 h for deposition temperatures 3, 30, and 80 °C, respectively. The thickness of prepared films according to SEM was a few hundred nanometers.

SEM images of CdSe films surface were obtained on Hitachi S 4800 field emission scanning electron microscope. TEM studies of CdSe nanoparticles were performed on LEO-906E transmission electron microscope. CdSe nanoparticles were carefully scraped from FTO substrate, ultrasonically dispersed in distilled water, and transferred to copper grids covered with collodion film for TEM measurements.

Photoelectrochemical measurements were fulfilled in a standard three electrode cell involving a platinum counter-electrode and an Ag|AgCl|KCl (sat.) electrode (+0.201 V vs standard hydrogen electrode (SHE)) as the reference one. All electrode potentials in the article are given with respect to SHE. Electrode potential was controlled with an Elins P-8 (Russia) potentiostat. Photocurrent spectra were obtained using a setup equipped with a high-intensity grating monochromator (spectral resolution 1 nm), a 250 W halogen lamp, and a light chopper. The spectral dependences of the incident photon-to-current conversion efficiency (IPCE, *Y*) were calculated from the photocurrent spectra and light intensity distribution at the monochromator output. Electrodes were illuminated from the conductive FTO substrate side to minimize the light absorption by electrolyte solutions. All solutions used were thoroughly purged with argon prior to and during the electrochemical and photoelectrochemical experiments.

XRD analysis was carried out with a Bruker D8 Advance diffractometer (Bragg-Brentano geometry, Cu K_α emission, 0.5°/min). Raman and PL spectra were measured at room temperature using a Nanofinder HE confocal spectrometer (LOTIS TII, Belarus-Japan) with 532 and 473 nm solid-state cw lasers as excitation sources. Incident optical power was attenuated to ≈20 μW to minimize a thermal impact. Backscattered light without analysis of its polarization was dispersed with a spectral resolution of 2.5 cm^{-1} (0.1 nm) and detected with a cooled CCD-matrix. Signal acquisition time was equal to 120 s. The excitation spot diameter was about 1 μm. Spectral calibration was done using a built-in gas-discharge lamp providing accuracy better than 2.5 cm^{-1} (0.1 nm). Rutherford backscattering spectrometry (RBS) was carried out using 1.3 MeV He^+ ions (scattering angle θ = 170°).

Results and discussion

XRD and optical characterization of CdSe films

CdSe films obtained at different deposition bath temperatures are characterized by a different color—from yellow to black-brown. Absorption spectra are shown in Fig. 1. There is a clear

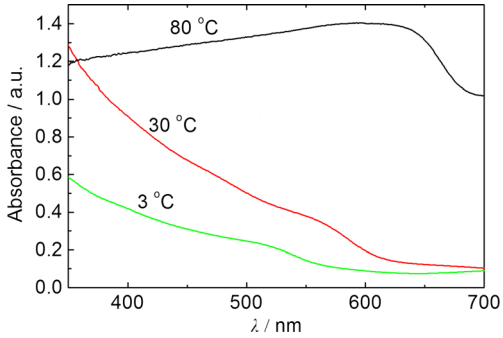

Fig. 1 Absorption spectra of the CdSe films deposited at 3, 30, and 80 °C

blue shift of the absorption edge with decreasing of deposition temperature. These results are fully consistent with previous studies [13–15] and are caused by synthesis of CdSe nanoparticles with different sizes and hence with different band gaps. It should also be noted that CdSe(80) demonstrates a pronounced light scattering.

SEM images of surface of prepared CdSe films are presented in Figs. 2a–c. The films are quite uniform, and sponge-like structure of CdSe(30) film can be seen. TEM images on Figs. 2d–f show that the films are composed of polydisperse nanoparticles. CdSe nanoparticles of several nanometers in diameter are predominant for CdSe(3) and CdSe(30) films, whereas for CdSe(80) significantly larger particles can be distinguished—10 nm and bigger. Nevertheless, it should be noted, that quantitative determination of nanoparticle diameter from TEM images is pretty difficult. Apparently, it is caused by the intimate contact of nanoparticles deposited by CBD which results in a continuous net of crystallites (aggregates) strongly bonded with each other. From one hand, it makes hard to distinguish a separate nanoparticle, but from the other hand, it provides an efficient transport of photogenerated charge carriers through the film. Thus, we have made a quantitative estimation of average diameter of nanoparticles prepared at different deposition temperature on the basis of photocurrent spectroscopy data (see below).

X-ray analysis shows that crystallinity of the CdSe films increases with the temperature of their deposition, as can be seen by an increase in the intensity of reflections and reduction of their width (Fig. 3a). It is known that cadmium selenide can crystallize both in hexagonal and cubic modifications [18]. In our case, the large width of the reflections for CdSe(3) and CdSe(30) does not allow determining the type of their crystal structure for sure, whereas CdSe(80) is clearly related to the hexagonal crystal modification.

Raman spectra of the films (Fig. 3b) have a band at 207 cm^{-1}, which corresponds to a scattering by longitudinal optical (LO) phonons in CdSe [18], as well as two of its overtones (2LO and 3LO). The increase of CdSe films deposition temperature leads to a gradual reduction in the width of the CdSe LO band (from 17 to 12 cm^{-1}), which is in agreement with improvement of crystallinity mentioned above. It may seem strange that there is no increase in the CdSe LO band intensity. However, this fact is naturally explained by a decrease of the band gap of CdSe, and an increase in the difference between its value and the photon energy (2.33 eV) used for excitation in Raman measurements. A similar effect was observed for the CdS nanoparticles with increasing of their size [19, 20].

As can be seen from Fig. 3c, PL spectra of the CdSe films deposited at low temperatures (CdSe(3) and CdSe(30)) have

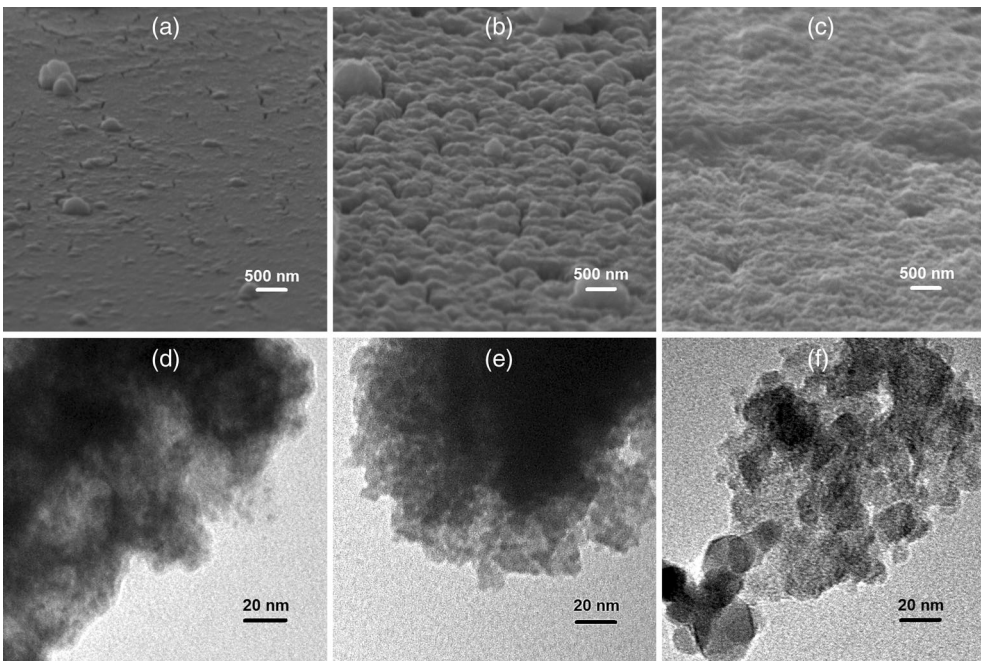

Fig. 2 SEM images of CdSe film surface (**a**–**c**) and TEM images of CdSe QDs. **a**, **d** CdSe(3). **b**, **e** CdSe(30). **c**, **f** CdSe(80)

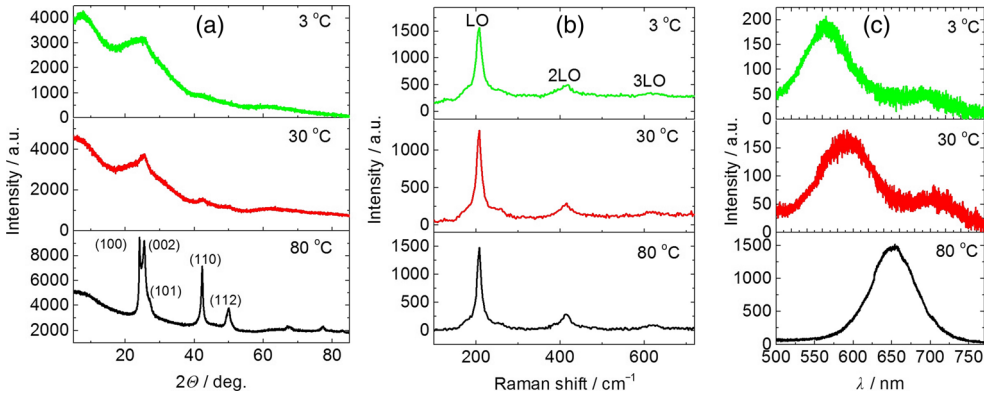

Fig. 3 X-ray diffraction patterns (**a**), Raman (**b**), and PL spectra (**c**) of CdSe films deposited at different deposition bath temperatures. Excitation 532 nm/20 μW (**b**); 473 nm/24 μW (**c**)

two bands. The position of the high-energy band enables one to associate it with the interband radiative recombination in the cadmium selenide nanoparticles, while the low-energy band corresponds to the radiative recombination through energy levels in the band gap of CdSe [21]. Raising the CdSe films deposition temperature from 3 to 80 °C leads to a shift of the interband radiative recombination band from 560 to 650 nm, which is in a qualitative agreement with the absorbance spectra (Fig. 1) and indicates a weakening of the quantum confinement in the CdSe nanoparticles. The disappearance of the low-energy component in the CdSe(80) PL spectra indicates the decrease of CdSe structural disorder with elevation of the deposition bath temperature correlating with a decrease in the spectral band width of interband radiative recombination, an increase in its intensity, as well as with the results of Raman and XRD analyzes.

Photoelectrochemical properties of CdSe films in Na_2SO_3 solution

CdSe QD films generate in Na_2SO_3 solution only anodic photocurrent under actinic illumination because this solution contains an effective acceptor of photoholes (sulfite anions), whereas there is no acceptor of photoelectrons (oxygen was removed by Ar purging). Thus, cadmium selenide demonstrates photoelectrochemical properties of *n*-type semiconductor: photoelectrons move through the nanoparticles into the conductive FTO substrate while photoholes oxidize sulfite anions.

Electron quantum-confinement effect for CdSe QD films is observed in the IPCE spectra (Fig. 4a). It is evident from the increase of the band gap (E_g) from 1.81 to 2.26 eV when the deposition temperature decreases from 80 to 3 °C (Table 1). The E_g values were determined by extrapolation of the linear part of the $(Yh\nu)^2$–$h\nu$ plot (direct optical transitions, Fig. 4b). As can be seen from Table 1, the nanoparticles average diameter (d) for CdSe(80) film estimated from E_g value [22, 23] increases more than twofold as compared to CdSe(3).

The deposition temperature affects not only the band gap of CdSe but also the value of IPCE (Fig. 4a). It was unexpected result that the maximum IPCE values are observed for CdSe(30), and minimal—for CdSe(80) films. The impact of various factors (particle size, film thickness, the depth of light penetration, etc.) on IPCE was analyzed earlier taking into account their influence on recombination as photocurrent loss mechanism [14, 15]. However, it will be demonstrated below that in our case there is an additional important factor affecting IPCE value—real surface area of CdSe film.

Photopolarization curves show that the anodic photocurrent saturates with the increase of anodic polarization of electrode, and the potential of photocurrent onset (E_{on}) takes more positive values with the increase in size of CdSe QDs (Fig. 5a). The observed $E_{on}(d)$ dependence can be explained in the following way. If the anodic photocurrent flows, the photoelectrons are transferred to the FTO substrate. Under the electrochemical polarization this process is possible if the Fermi level of the conductive glass is more positive than the electron quasi-Fermi level (E_{Fn}) of CdSe, which is usually considered as located close to conduction band edge (E_c). Hence, while shifting the Fermi level of the FTO substrate up during the cathodic scan of electrode potential, one should observe the disappearance of photocurrent when it reaches E_c of CdSe nanoparticles [24]. Therefore, the observed cathodic shift of E_{on} with decrease of CdSe QD size indicates shift of their E_c to a higher energy. We have used the E_{on} values to estimate the position of the conduction band edge of CdSe nanoparticles depending on their size. For CdSe(3) nanoparticles with 4 nm average diameter, the conduction band potential was estimated to be −0.75 V (Fig.5b). The conduction band shifts to positive potentials with the increase of particles size (−0.57 V for 5 nm particles and −0.23 V for 10 nm particles). The position of the valence band (E_v) was determined based on the E_c and E_g values. Figure 5b shows clearly that the reduction of particles size influences on the position of E_c much stronger than on E_v. In other words, most of the band gap increase is due to the shift of the conduction band edge to more negative potentials. This situation is typical for CdSe

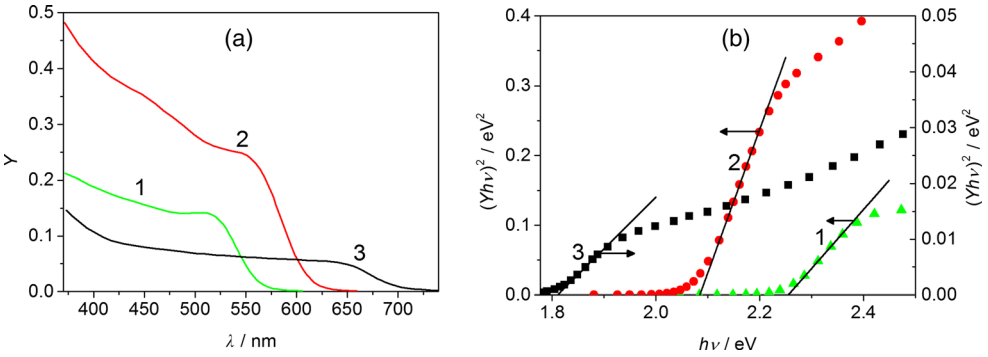

Fig. 4 Spectra of anodic photocurrent in $Y - \lambda$ (**a**) and $(Y \times h\nu)^2 - h\nu$ (**b**) coordinates: *1* CdSe(3), *2* CdSe(30), and *3* CdSe(80). The solution is 0.1 M Na_2SO_3. Applied potential is 0.2 V

[25, 26], as well as for CdS [27], CdTe [28], and ZnO [29] QDs and is naturally attributed to a significant difference in the effective masses of electrons and holes.

Note that the obtained E_c and E_v values are anodically shifted by appr. 0.5 V in comparison with the values provided by theoretical calculations [30] and experimental findings (ultraviolet photoelectron emission spectroscopy [31–33], cyclic voltammetry in non-aqueous solutions [34–36]). Such discrepancy could be explained by (i) impact of recombination [24], (ii) influence of specific adsorption of ions and dipoles of solvent [31], and (iii) non-negligible difference between E_c and E_{Fn} for CdSe QDs. Nevertheless, the obtained constancy in E_v position regardless of the CdSe QD size is in a good agreement with the above-cited works [30–36].

The energy level corresponding to standard redox potential of the SO_4^{2-}/SO_3^{2-} redox system (−0.47 V, pH 9.3) is located far enough from the valence band of CdSe (even if E_c and E_v have more negative potentials in comparison with the data presented in Fig. 5b). Thus, the size of the nanoparticles should have no influence on the rate of photoelectrochemical oxidation process, as the photoholes generated in the valence band have a sufficient energy for injection into electrolyte from particles of any size. Therefore, we can assume that high quantum efficiency for the anodic photoelectrochemical process which takes place on the surface of nanocrystalline CdSe films can be achieved not by means of the band-edge tuning of cadmium selenide quantum dot particles but primarily due to an effective charge separation at the semiconductor-electrolyte interface. Thereby, we need to have information about the real surface area of photoelectrodes and an appropriate method for its evaluation.

Table 1 Band gap (E_g), average particle diameter (d), and onset potential (E_{on}) for CdSe QDs deposited at different temperatures

QD film	E_g, eV	d, nm	E_{on}, V 0.1 M Na_2SO_3
CdSe(3)	2.26	4	−0.75
CdSe(30)	2.09	5	−0.57
CdSe(80)	1.81	10	−0.23

Cadmium underpotential deposition on CdSe QD films

To estimate the real surface area of the CdSe QD films, the cadmium UPD process was used. Classically, UPD involves deposition of a less noble element (most often, metal) on a more noble substrate and is limited to the formation of 2D atomic layers (monolayers) [37–39]. The phenomenon of Cd UPD on CdSe is well-documented [40–43]. It involves the deposition of Cd atomic layers on Se atoms in the crystal lattice of CdSe at a potential prior to (under) that required for deposition of the Cd on itself and is widely used for the electrosynthesis of CdSe in the electrochemical atomic layer epitaxy (ECALE) method [44]. Since UPD is a surface-limited process, the passed electrical charge makes it possible to estimate the real electrode surface area (roughness factor—*f*) assuming the formation of cadmium adatoms monolayer [45].

Cyclic voltammograms (CVA) of Cd^{2+} cathodic reduction and anodic oxidation of metal (Cd^0) for the CdSe(30) electrode are shown in Fig. 6. CVA for CdSe(3) and CdSe(80) are qualitatively similar.

The equilibrium redox potential $E(Cd^{2+}/Cd^0)$ calculated according to the Nernst equation is −0.48 V. There is no cathodic current in the solution which contains no Cd^{2+} cations (0.1 M Na_2SO_4, pH 4) in the studied potential range (Fig. 6, curve 1). Therefore, the cathodic current observed during the cathodic scan at $E > E(Cd^{2+}/Cd^0)$ is associated with the cadmium UPD process.

The formation of metal phase occurs at $E < -0.60$ V (Fig. 6, curves 3, 4), i.e., is characterized by a sufficiently large (0.12 V) overvoltage. Bulk cadmium is oxidized at the anodic scan of potential giving the characteristic anodic current peak. It should be noted that in contrast to the bulk metal, cadmium adatoms are not oxidized during the anodic scan (Fig. 6, curve 2), i.e., the UPD is irreversible. Thus, the cadmium UPD on the CdSe QD electrodes can be carried out only once. As a result, CdSe surface becomes enriched with cadmium atoms (Cd-terminated surface).

Assuming that the surface concentration of cadmium adatoms in the monolayer is about 10^{15} at/cm^2, we can estimate the amount of charge required for its formation.

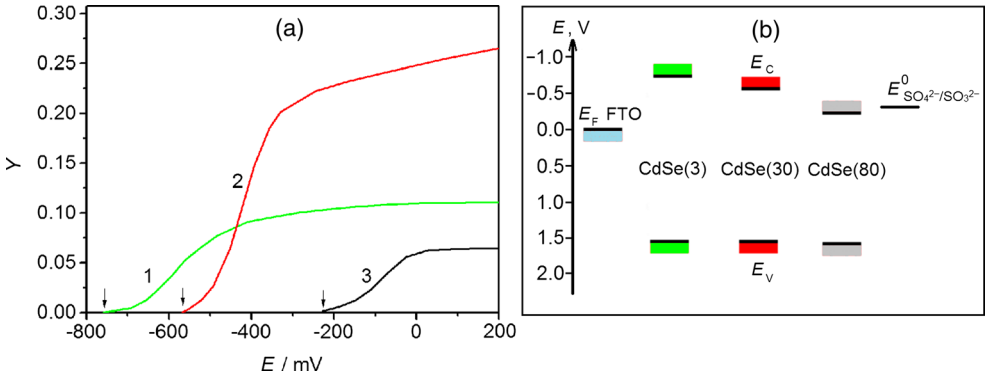

Fig. 5 **a** The dependences of IPCE on electrode potential: *1* CdSe(3), 2 CdSe(30), and 3 CdSe(80); excitation light wavelength 530 nm; solution 0.1 M Na_2SO_3. **b** Energy diagram for CdSe QDs of different sizes in Na_2SO_3 solution

Considering that the reduction of Cd^{2+} cation requires two electrons, we can get a charge of 0.32 mC/cm^2. The charges under the cathodic potentiodynamic curves (calculated up to the potential of the metal phase formation −0.60 V), and the factors of electrode surface roughness *f* are shown in Table 2. The obtained *f* values suggest that the CBD CdSe films have an extremely large real surface area, which is 1–2 orders of magnitude (!) greater than the geometric surface area of the electrode. The largest area of contact with electrolyte solution is observed for CdSe(30) which correlates with the largest anodic IPCE values for these films (Fig. 4a) and their globular structure (Fig. 2b).

Cathodic photocurrent in polyselenide solution

It is well known that CdSe QDs have high quantum efficiency and photocorrosion stability in the polysulfide electrolyte [46]. Photocurrent switching for CdSe was observed in this electrolyte after etching in dilute HCl [15, 17]. However, we declined purposely to use this electrolyte because it was clearly proved that the surface of CdSe changes its chemical composition forming a CdS/CdSe heterojunction in this solution [12, 46].

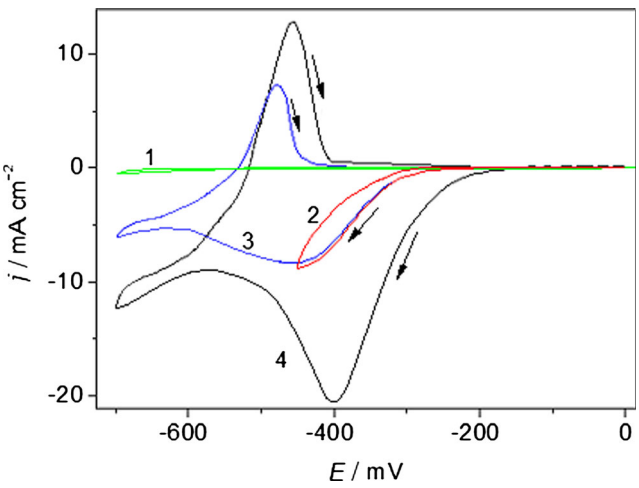

Fig. 6 Cyclic voltammograms for CdSe(30): *1* in the solution of 0.1 M Na_2SO_4 (pH 4); *2–4* in the solution of 0.01 M $CdSO_4$ + 0.1 N Na_2SO_4 (pH 4). The solutions were saturated with Ar. 1–3 as-deposited, *4* after selenization. Potential scan rate is 50 mV/s

For cathodic photocurrent investigation, we have used the polyselenide electrolyte containing 0.02 M Se, 10 M NaOH, 0.2 M Na_2SO_3, and 0.1 M Na_2SeSO_3. Selenide (Se^{2-}) and polyselenide (Se_n^{2-}) are formed by the following reactions:

$$3Se + 6OH^- = 2Se^{2-} + SeO_3^{2-} + 3H_2O,$$
$$(n-1)Se + Se^{2-} = Se_n^{2-}.$$

Concentrated alkali solution is necessary for efficient elemental selenium disproportionation, as well as for suppressing of the hydrolysis reactions. In this case, we are dealing with a reversible redox system with both the acceptor of photoholes (Se^{2-}) and photoelectrons acceptor (Se_n^{2-}). It allows us to study the effect of photocurrent switching (changing its sign). Photocorrosion stability of CdSe QD electrodes in this electrolyte is sufficiently high. It is essential to minimize the effects associated with nanoparticles photocorrosion, dissolving, and, consequently, changing of their size.

Na_2SO_3 and Na_2SeSO_3 were also added to the electrolyte. Firstly, SO_3^{2-} and $SeSO_3^{2-}$ anions along with Se^{2-} are effective photoholes scavengers. Secondly, sulfite removes traces of molecular oxygen from the solution, and $SO_3^{2-}/SeSO_3^{2-}$ pair prevents precipitation of elemental selenium by its binding in selenosulfate.

There is a significant change in PEC behavior of the CdSe QD films in polyselenide electrolyte as compared to Na_2SO_3 solution. Photopolarization curves in Fig. 7 obtained by subtracting the dark current from the total current observed under illumination demonstrate that the CdSe electrodes generate cathodic

Table 2 The charge of UPD deposited cadmium adatoms (Q_{UPD}) and the roughness factor (*f*) for the CdSe films obtained at different deposition bath temperatures; solution contains 0.01 M $CdSO_4$ + 0.1 M Na_2SO_4, pH 4

QD film	Q_{UPD}, mC/cm^2	*f*
CdSe(3)	4.4	14
CdSe(30)	40.1	125
CdSe(80)	2.7	8

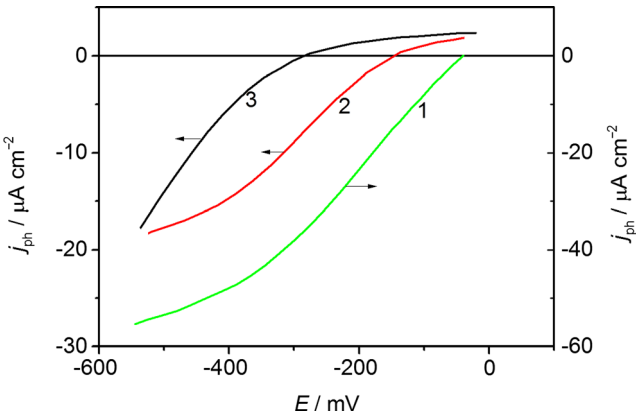

Fig. 7 The dependences of photocurrent density on the electrode potential for CdSe QD electrodes it the solution containing 0.02 M Se, 10 M NaOH, 0.2 M Na_2SO_3, 0.1 M Na_2SeSO_3. *1* CdSe(3), *2* CdSe(30), and *3* CdSe(80). Excitation light wavelength is 530 nm (J = 800 μW/cm^2). Potential scan rate is 5 mV/s

photocurrent. *P*-type behavior means preferential photoelectron injection into the electrolyte. The effect of photocurrent switching is the most pronounced for CdSe(3) electrodes – in polyselenide electrolyte these electrodes demonstrate only cathodic photocurrent with the largest IPCE (Fig. 7). Cathodic photocurrent for CdSe(30) and CdSe(80) films is also dominant, but a minor anodic photocurrent can be detected as well. Furthermore, if on CdSe(3) cathodic photocurrent is registered immediately after immersion into the polyselenide electrolyte, for CdSe(30), just after the immersion of electrode into the electrolyte, a decreasing anodic photocurrent is observed and switching to cathodic photocurrent occurs after 10 s of contact with the electrolyte; for CdSe(80), photocurrent switching is observed only after 10–15 min. Such delay in appearance of cathodic photocurrent means that the presence of electron acceptor species in electrolyte is not enough for electron injection into solution and surface modification is necessary. It is logical to assume that photocurrent switching is related to enrichment of CdSe surface with selenium (Se-terminated surface). Se-terminated surface formation occurs due to the chemisorption of Se^{2-} and Se_n^{2-} on the surface of CdSe. This process is identical to the well known SILAR method used for CdSe nanoparticles synthesis [47]. The obtained results indicate a high rate of Se^{2-} and Se_n^{2-} chemisorption on the CdSe particles of a small size.

As a result of the formation of Se-terminated surface, the concentration of selenium surface atoms on CdSe nanoparticles increases. In order to verify this claim, cadmium UPD was carried out on the CdSe electrodes with Se-terminated surface. CdSe films treated in polyselenide electrolyte for 10 s and washed with 10 M alkali (to prevent hydrolysis) and distilled water were immersed in a solution containing Cd^{2+} cations. Charges corresponding to the cathodic peaks (Q_{UPD}) on CdSe electrodes with Se-terminated surface are shown in Table 3. A significant increase in Q_{UPD} values is observed for all CdSe films after surface selenization. The observed increase in the real

Table 3 Band gap (E_g), band gap decrease (ΔE_g), the charge of UPD deposited cadmium adatoms (Q_{UPD}) and the roughness factor (f) for the CdSe films with Se-terminated surface; solution for UPD experiments contains 0.01 M $CdSO_4$ + 0.1 M Na_2SO_4, pH 4

QD film	E_g, eV	ΔE_g, eV	Q_{UPD}, mC/cm^2	f
CdSe(3)	2.08	0.18	8.4	26
CdSe(30)	2.00	0.09	87.6	274
CdSe(80)	1.81	0	4.5	14

surface for selenized CdSe QD films can be attributed to an increase in the concentration of selenium surface atoms on CdSe nanocrystals, as well as to an increase in the size of QDs due to the chemisorption of Se^{2-} and Se_n^{2-}.

An additional direct evidence of Se concentration increase in the films after their treatment in the polyselenide electrolyte was obtained using RBS. As it is seen in Fig. 8, immersion in polyselenide electrolyte does not affect position of the Cd-related high-energy peak indicating that no bulk selenium is formed on the electrode surface. At the same time, one can observe an enhancement of relative intensity of the Se-related peak and its low-energy broadening, which points to increase of selenium content in the film.

The growth of the CdSe QDs size as a result of selenization of the films is also proved by the cathodic photocurrent spectra (Fig. 9). The band gap estimated from the photocurrent spectra after surface selenization is reduced by 0.18 eV for CdSe(3) and 0.09 eV for CdSe(30), remaining unchanged for CdSe(80) (Table 3).

As can be seen from Fig. 9 (curve 1), the largest quantum efficiency of cathodic photocurrent is observed for CdSe(3), i.e., for QDs with minimal size. The equilibrium potential of the Se_n^{2-}/Se^{2-} redox system measured on Pt-electrode is −0.35 V. Therefore, $E(Se_n^{2-}/Se^{2-})$ is located closely to the

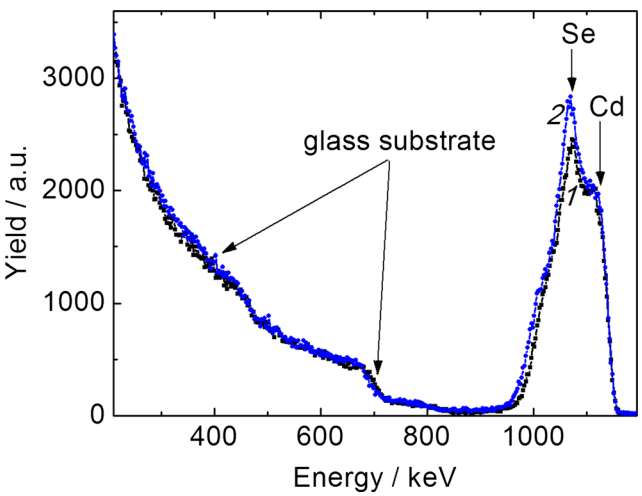

Fig. 8 Rutherford backscattering spectra of CdSe(3) film before (*1*) and after (*2*) treatment in the polyselenide electrolyte

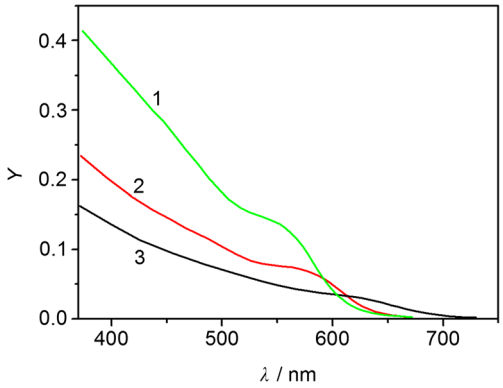

Fig. 9 IPCE spectra of cathodic photocurrent for CdSe electrodes in polyselenide electrolyte at applied potential of −0.5 V. *1* CdSe(3), *2* CdSe(30), and *3* CdSe(80)

conduction band edge of CdSe. Thus, small CdSe quantum dots with their increased band gaps have more favorable conduction band energies for injecting photoelectrons to polyselenide anions. In this case, we observe size-dependent electron injection from CdSe quantum dots into electrolyte. A similar situation was observed when the injection of photoelectrons occurred from excited CdSe quantum dots into TiO_2 nanoparticles [23].

Recombination losses of photogenerated charges in nanocrystalline CdSe films occur at interparticle boundaries, as well as are associated with possibility of indirect recombination by electron and hole injection into the electrolyte. The latter one can take up to 30–40 % of total efficiency [15] and is related to the parallel passing of associated photoelectrochemical oxidation and reduction reactions [16, 48, 49]. Change of photocurrent sign for CdSe(30) and CdSe(80) electrodes occurs under electrochemical polarization (Fig. 7) and the potential of photocurrent switching (E_{sw}) correlates with the equilibrium potential of the Se_n^{2-}/Se^{2-} redox system. A similar effect was observed earlier for nanocrystalline BiOI electrodes [50]. It was shown [50] that when electrode potential is equal to E_{sw}, photocurrent is absent due to the recombination of photoholes and photoelectrons with the redox system components, and the value E_{sw} is determined by equality of exchange currents of anodic and cathodic processes.

It should be noted, that photocurrent switching effect has been already described in the literature for individual semiconductor electrodes [50, 51], as well as for semiconductor heterostructures [52, 53]. This effect can be applied in novel logical nanoswitchers [52].

Conclusions

Photoelectrochemical behavior of the chemical bath deposited CdSe QD films was investigated. Varying of the deposition bath temperature from 3 to 80 °C resulted in the change of CdSe nanoparticles average diameter from 4 to 10 nm and the band gap from 2.26 to 1.81 eV. In aqueous Na_2SO_3 solution (without dissolved oxygen), the CdSe photoelectrodes generate only anodic photocurrent (*n*-type behavior), whereas a gradual change of photocurrent from anodic to cathodic occurs after immersion of the films in polyselenide electrolyte containing Se_n^{2-}/Se^{2-} redox couple. The appearance of cathodic photocurrent is related to Se-termination of the CdSe surface as it was demonstrated by the cadmium underpotential deposition on CdSe treated with the polyselenide electrolyte. The effect of photocurrent switching depends on the particle size and is most pronounced for CdSe QDs with the minimal size (d = 4 nm) due to more favorable conduction band energies for injecting electrons into Se_n^{2-} anions. On the contrary, for photoholes injection in the electrolyte (anodic photocurrent) this fact is not important, because the position of the valence band does not vary with the size of the particles.

Cadmium UPD on CdSe was used to evaluate in situ the real surface area of the photoelectrodes, which has turned to be 1–2 orders of magnitude higher than the geometrical surface area. High quantum efficiency of photoelectrochemical processes (IPCE ~40 %) in the nanocrystalline CdSe photoelectrodes is provided by an effective charge separation at the highly developed semiconductor-electrolyte interface.

Acknowledgments This work was supported by project no. 2/217/GF4 within the state program no. 055 "Scientific and/or scientific and technical activity" (subprogram 101) of the Republic of Kazakhstan.

References

1. Kamat P (2008) Quantum dot solar cells. Semiconductor nanocrystals as light harvesters. J Phys Chem C 112:18737–18753
2. Alivisatos AP (1996) Semiconductor clusters, nanocrystals, and quantum dots. Science 271:933–937
3. Nozik AJ (2002) Quantum dot solar cells. Phys E 14:115–120
4. Rühle S, Shalom M, Zaban A (2010) Quantum-dot-sensitized solar cells. ChemPhysChem 11:2290–2304
5. Hetsch F, Xu X, Wang H, Kershaw SV, Rogach AL (2011) Semiconductor nanocrystal quantum dots as solar cell components and photosensitizers: material, charge transfer, and separation aspects of some device topologies. J Phys Chem Lett 2:1879–1887
6. Kryukov AI, Stroyuk OL, Kuchmiy SY, Pohodenko VD (2013) Nanophotocatalysis. Akademperiodika, Kiev
7. Bard AJ (1979) Photoelectrochemistry and heterogeneous photocatalysis at semiconductors. J Photochem 10:59–75
8. Kamat PV (2012) Manipulation of charge transfer across semiconductor interface. A criterion that cannot be ignored in photocatalyst design. J Phys Chem Lett 3:663–672
9. Vaneski A, Schneider J, Susha AS, Rogach AL (2014) Aqueous synthesis of CdS and CdSe/CdS tetrapods for photocatalytic hydrogen generation. APL Mater 2:012104
10. Gaponenko SV (2010) Introduction to nanophotonics. Cambridge University Press, Cambridge
11. Talapin DV, Lee JS, Kovalenko MV, Shevchenko EV (2010) Prospects of colloidal nanocrystals for electronic and optoelectronic applications. Chem Rev 110:389–458

12. Bang JH, Kamat PV (2009) Quantum dot sensitized solar cells. A tale of two semiconductor nanocrystals: CdSe and CdTe. ACS Nano 3:1467–1476
13. Hodes G (2007) Semiconductor and ceramic nanoparticle films deposited by chemical bath deposition. Phys Chem Chem Phys 9: 2181–2196
14. Hodes G, Albu-Yaron A, Decker F, Motisuke P (1987) Three-dimensional quantum-size effect in chemically deposited cadmium selenide films. Phys Rev B 36:4215–4221
15. Hodes G, Howell ID, Peter LM (1992) Nanocrystalline photoelectrochemical cells. A new concept in photovoltaic cells. J Electrochem Soc 139:3136–3140
16. Hagfeldt A, Grätzel M (1995) Light-induced redox reactions in nanocrystalline systems. Chem Rev 95:49–68
17. Kronik L, Ashkenasy N, Leibovitch M, Fefer E, Shapira Y, Gorer S, Hodes G (1998) Surface states and photovoltaic effects in CdSe quantum dot films. J Electrochem Soc 145:1748–1755
18. Madelung O (2004) Semiconductors: data handbook. Springer-Verlag, Berlin – Heidelberg
19. Malashchonak MV, Mazanik AV, Korolik OV, Streltsov EA, Kulak AI (2015) Influence of wide band gap oxide substrates on the photoelectrochemical properties and structural disorder of CdS nanoparticles grown by the successive ionic layer adsorption and reaction (SILAR) method. Beilstein J Nanotechnol 6:2252–2262
20. Kozitskiy AV, Stroyuk OL, Kuchmiy SY, Mazanik AV, Poznyak SK, Streltsov EA, Kulak AI, Korolik OV, Dzhagan VM (2014) Photoelectrochemical and Raman characterization of nanocrystalline CdS grown on ZnO by successive ionic layer adsorption and reaction method. Thin Solid Films 562:56–62
21. Qu L, Peng X (2002) Control of photoluminescence properties of CdSe nanocrystals in growth. J Am Chem Soc 124:2049–2055
22. Efros AL, Efros AL (1982) Interband light absorption in semiconductor sphere. Soviet Physics Semiconductors 16:772–775
23. Robel I, Kuno M, Kamat PV (2007) Size-dependent electron injection from excited CdSe quantum dots into TiO_2 nanoparticles. J Am Chem Soc 129:4136–4137
24. Beranek R (2011) (Photo)electrochemical methods for the determination of the band edge positions of TiO_2-based nanomaterials. Advances in Physical Chemistry 2011:786759
25. Norris DJ, Bawendi MG (1996) Measurement and assignment of the size-dependent optical spectrum in CdSe quantum dot. Phys Rev B 53:16338–16346
26. Wang C, Shim M, Guyot-Sionnest P (2001) Electrochromic nanocrystal quantum dots. Science 291:2390–2392
27. Miyake M, Torimoto T, Sakata T, Mori H, Yoneyama H (1999) Photoelectrochemical characterization of nearly monodisperse CdS nanoparticles-immobilized gold electrodes. Langmuir 15: 1503–1507
28. Rajh T, Mićić OI, Nozik AJ (1993) Synthesis and characterization of surface-modified colloidal CdTe quantum dots. J Phys Chem 97: 11999–12003
29. Jacobsson TJ, Edvinsson T (2012) Photoelectrochemical determination of the absolute band edge positions as a function of particle size for ZnO quantum dots. J Phys Chem C 116:15692–15701
30. Wang LW, Zunger A (1996) Pseudopotential calculations of nanoscale CdSe quantum dots. Phys Rev B 53:9579–9582
31. Jasieniak J, Califano M, Watkins SE (2011) Size-dependent valence and conduction band-edge energies of semiconductor nanocrystals. ACS Nano 5:5888–5902
32. Markus TZ, Wu M, Wang L, Waldeck DH, Oron D, Naaman R (2009) Electronic structure of CdSe nanoparticles adsorbed on Au electrodes by an organic linker: Fermi level pinning of the HOMO. J Phys Chem C 113:14200–14206
33. Meulenberg RW, Lee JR, Wolcott A, Zhang JZ, Terminello LJ, Buuren T (2009) Determination of the exciton binding energy in CdSe quantum dots. ACS Nano 3:325–330
34. Inamdar SN, Ingole PP, Haram SK (2008) Determination of band structure parameters and the quasi-particle gap of CdSe quantum dots by cyclic voltammetry. ChemPhysChem 9:2574–2579
35. Querner C, Reiss P, Sadki S, Zegorska M, Pron A (2005) Size and ligand effects on the electrochemical and spectroelectrochemical responses of CdSe nanocrystals. Phys Chem Chem Phys 7:3204–3209
36. Kucur E, Riegler J, Urban GA, Nann T (2003) Determination of quantum confinement in CdSe nanocrystals by cyclic voltammetry. J Chem Phys 119:2333–2337
37. Herrero E, Buller LJ, Abruna HD (2001) Underpotential deposition at single surfaces of Au, Pt, Ag and other materials. Chem Rev 101: 1897–1930
38. Kolb DM (1978) In: Gerischer H, CW T (eds) Advances in electrochemistry and electrochemical engineering, vol Vol 11. Wiley, New York
39. Chulkin PV, Aniskevich YM, Streltsov EA, Ragoisha GA (2015) Underpotential shift in electrodeposition of metal adlayer on tellurium and the free energy of metal telluride formation. J Solid State Electrochem 19:2511–2516
40. Ragoisha GA, Streltsov EA, Rabchynski SM, Ivanou DK (2011) Cadmium cathodic deposition on polycrystalline p-selenium: dark and photoelectrochemical processes. Electrochim Acta 56:3562–3566
41. Mathe MK, Cox SM, Flowers BH, Vaidyanathan R, Pham L, Srisook N, Happek U, Stickney JL (2004) Deposition of CdSe by EC-ALE. J Crystal Growth 271:55–64
42. Colletti LP, Flowers BH, Stickney JL (1998) Formation of thin films of CdTe, CdSe, and CdS by electrochemical atomic layer epitaxy. J Electrochem Soc 145:1442–1449
43. Lister TE, Stickney JL (1996) Formation of the first monolayer of CdSe on Au(111) by electrochemical ALE. Appl Surf Sci 107:153–160
44. Gregory BW, Stickney JL (1991) Electrochemical atomic layer epitaxy (ECALE). J Electroanal Chem 300:543–561
45. Trasatti S, Petrii OA (1992) Real surface area measurements in electrochemistry. J Electroanal Chem 327:353–376
46. Chakrapani V, Baker D, Kamat PV (2011) Understanding the role of the sulfide redox couple (S^{2-}/S_n^{2-}) in quantum dot-sensitized solar cells. J Am Chem Soc 133:9607–9615
47. Pathan HM, Lokhande CD (2004) Deposition of metal chalcogenide thin films by successive ionic layer adsorption and reaction (SILAR) method. Bull Mater Sci 27:85–111
48. Bard AJ (1982) Design of semiconductor photoelectrochemical systems for solar energy conversion. J Phys Chem 86:172–177
49. Solarska R, Rutkowska I, Morand R, Augustynski J (2006) Photoanodic reactions occurring at nanostructured titanium dioxide films. Electrochim Acta 51:2230–2236
50. Kazyrevich ME, Malashchonak MV, Mazanik AV, Streltsov EA, Kulak AI, Bhattacharya C (2016) Photocurrent switching effect on platelet-like BiOI electrodes: influence of redox system, light wavelength and thermal treatment. Electrochim Acta 190:612–619
51. Podborska A, Gawel B, Pietrzak L, Szymanska IB, Jeszka JK, Lasocha W, Szaciłowski K (2009) Anomalous photocathodic behavior of CdS within the Urbach tail region. J Phys Chem C 113: 6774–6784
52. Long M, Beranek R, Cai W, Kisch H (2008) Hybrid semiconductor electrodes for light-driven photoelectrochemical switches. Electrochim Acta 53:4621–4626
53. Bai Z, Zhang Y (2016) Self-powered UV266a 53:4photodetectors based on ZnO/Cu_2O nanowire/electrolyte heterojunctions. J Alloys Compd 675:325–330